Published in final edited form as:
J Neurophysiol. 2007 January ; 97(1): 296–306. doi:10.1152/jn.00823.2006.

Complementary Postsynaptic Activity Patterns Elicited in Olfactory Bulb by Stimulation of Mitral/Tufted and Centrifugal Fiber Inputs to Granule Cells

Nora Laaris[1], **Adam Puche**[2], and **Matthew Ennis**[3]

[1]Department of Pharmacology and Experimental Therapeutics, University of Maryland, Baltimore, Maryland [2]Department of Anatomy and Neurobiology, University of Maryland, Baltimore, Maryland [3]Department of Anatomy and Neurobiology, University of Tennessee Health Science Center, Memphis, Tennessee

Abstract

Main olfactory bulb (MOB) granule cells receive spatially segregated glutamatergic synaptic inputs from the dendrites of mitral/tufted cells as well as from the axons of centrifugal fibers (CFFs) originating in olfactory cortical areas. Dendrodendritic synapses from mitral/tufted cells occur on granule cell distal dendrites in the external plexiform layer (EPL), whereas CFFs preferentially target the somata/proximal dendrites of granule cells in the granule cell layer (GCL). In the present study, tract tracing, and recordings of field potentials and voltage-sensitive dye optical signals were used to map activity patterns elicited by activation of these two inputs to granule cells in mouse olfactory bulb slices. Stimulation of the lateral olfactory tract (LOT) produced a negative field potential in the EPL and a positivity in the GCL. CFF stimulation produced field potentials of opposite polarity in the EPL and GCL to those elicited by LOT. LOT-evoked optical signals appeared in the EPL and spread subsequently to deeper layers, whereas CFF-evoked responses appeared in the GCL and then spread superficially. Evoked responses were reduced by *N*-methyl-D-aspartate (NMDA) receptor antagonists and completely suppressed by AMPA receptor antagonists. Reduction of extracellular Mg^{2+} enhanced the strength and spatiotemporal extent of the evoked responses. These and additional findings indicate that LOT- and CFF-evoked field potentials and optical signals reflect postsynaptic activity in granule cells, with moderate NMDA and dominant AMPA receptor components. Taken together, these results demonstrate that LOT and CFF stimulation in MOB slices selectively activate glutamatergic inputs to the distal dendrites versus somata/proximal dendrites of granule cells.

INTRODUCTION

Granule cells of the main olfactory bulb (MOB) are regulated by two primary classes of excitatory afferent inputs. Within the external plexiform layer (EPL), the distal dendrites of granule cells receive dendrodendritic input from mitral/tufted cells. Extrinsic centrifugal fiber (CFF) projections to MOB arise from nearly all of the primary olfactory cortical structures targeted by the outputs of mitral/tufted cells, including the anterior olfactory nucleus (AON), and piriform, periamygdaloid and lateral entorhinal cortex (for review, see Ennis et al. 2006). The somata and proximal dendrites of granule cells are preferentially targeted by these extrinsic

Address for reprint requests and other correspondence: M. Ennis, Dept. of Anatomy and Neurobiology, University of Tennessee Health Science Center, 855 Monroe Ave., Suite 515, Memphis, TN 38163 (mennis@utmem.edu)..

excitatory centrifugal inputs (Davis and Macrides 1981; Luskin and Price 1983; Price and Powell 1970).

Mitral/tufted to granule cell dendrodendritic synaptic transmission has been extensively studied. Glutamate released from mitral cell dendrites activates both AMPA and *N*-methyl-D-aspartate NMDA) receptors on granule cell spines, although the NMDA receptor plays a dominant role in regulating granule cell GABA release (Aroniadou-Anderjaska et al. 1999; Chen et al. 2000; Halabisky et al. 2000; Isaacson and Strowbridge 1998; Schoppa et al. 1998). Functionally, granule cell-mediated dendritic inhibition is thought to play a major role in infraglomerular circuits that sharpen contrast among odorant representations arising from populations of mitral cells associated with different glomeruli and thus receiving input from olfactory sensory neurons with different odorant response specificities (Luo and Katz 2001; Yokoi et al. 1995).

By contrast, comparatively less is known about the properties and functional role of extrinsic CFF input to granule cells. Projections from primary olfactory cortical structures form asymmetrical (i.e., presumably excitatory) synapses on granule cell bodies and dendrites (Price and Powell 1970). Activation of primary olfactory cortical structures, or stimulation of the anterior commissure, which is a major route for centrifugal projections to MOB, produces a negative field potential in the granule cell layer (GCL) as expected if excitatory currents are flowing into granule cells (Mori and Takagi 1978; Nakashima et al. 1978; Neville and Haberly 2003; Nickell and Shipley 1993; Patneau and Stripling 1992; Stripling et al. 1991). Cellular recording studies in vivo demonstrate that similar stimulation produces spikes or excitatory postsynaptic potentials (EPSPs) in granule cells, followed by inhibitory postsynaptic potentials (IPSPs) in mitral cells (Mori and Takagi 1978; Nakashima et al. 1978; Nicoll 1971; Yamamoto et al. 1963). Other important aspects of CFF regulation of granule cells remain unanswered. For example, CFF projections from some divisions of the AON selectively target the distal dendrites of granule cells in the EPL (Davis and Macrides 1981; Luskin and Price 1983). The relative strength of inputs to the proximal versus distal dendrites of granule cells is unknown. The role of ionotropic glutamate receptor subtypes in centrifugal synaptic transmission to granule cells has not been investigated.

Experiments to address many of these questions are most amenable in slice preparations. At the caudal pole of the MOB, the anterior commissure and LOT are located at equivalent rostrocaudal and dorsoventral levels and thus may be preserved in in vitro horizontal slices commonly used for MOB electrophysiology. The goal of the this study was to use field potential and voltage-sensitive dye (VSD) optical recordings to investigate postsynaptic activity patterns and the involvement of ionotropic glutamate receptors in responses elicited by focal activation of centrifugal inputs to granule cells in mouse olfactory bulb slices. The specificity of the centrifugal-evoked responses was assessed by comparing them to those elicited by antidromic activation of mitral/tufted dendrodendritic inputs to granule cells.

METHODS

Tract tracing

Animal protocols used in this study complied with institutional and federal regulations. Young or adult (19- to 60-day old) C57BL/6J mice (Jackson Laboratory, Bar Harbor, ME) were anesthetized with sodium pentobarbital (100 mg/kg) and transcardially perfused with 4% paraformaldehyde in 0.1M phosphate buffer. The brains (n = 3) were removed, and a coronal cut was made at the level of the caudal AON with a tungsten carbide razor blade. This cut permitted visual observation of the white matter of both the CFF tract and the LOT. A crystal of 4-(4-(dihexadecylamino)styryl-*N*-methylpyridinium iodine (DiA) was inserted into the white matter CFF tract, and a 1,1′-dioctadecyl-3,3,3′,3′-tetramethylindocarbocyanine

perchlorate (DiI) crystal was inserted into the LOT on the lateral surface of the brain visualized under oblique reflected illumination. The DiI crystal inserted into the LOT could result in labeling of pyramidal neurons in the PC via contacts with their dendrites in layer Ib and thus cross-label the CFFs. To prevent this aberrant cross-labeling, a shallow tangential cut was made through layer II of the cortex between the DiA and DiI crystal placements to isolate pyramidal cell dendrites in layer 1b from pyramidal soma/axons in layers II/II and the CFFs. The brains were incubated at 32°C for 4 wk, vibratome sectioned, mounted onto slides with a DABCO-based anti-fading agent, and viewed on an Olympus FluoView confocal microscope. To correlate the position and distribution of CFF and LOT axons with the slice electrophysiology experiments, we implanted DiI in the CFF tract and DiA in the LOT in 400-μM-thick, quasi-horizontal slices (n = 4 slices, procedures in the following text). Slices were processed, mounted, counterstained with the nuclear dye DAPI and then analyzed as described in the preceding text.

In vitro slice preparation

Mice (19- to 28-day old) were anesthetized (pentobarbital, 100 mg/kg ip), and the olfactory bulbs and a portion of the rostral forebrain were removed. Horizontal slices (400-μm-thick) were harvested as previously described (Heinbockel et al. 2004) with the following modifications to optimally preserve the CFF tract and the rostral component of the LOT. The MOB-rostral forebrain block was secured, ventral side down, to a custom fabricated chuck (designed for the standard tissue pedestal of the Electron Microscopy Sciences Model OTS-4000 vibratome, Hatfield, PA); this allowed for rotation of the MOB-rostral forebrain block in two dimensions. The block was oriented with the long rostrocaudal axis parallel to vibratome cutting path. The block was then rotated along the rostrocaudal axis to lower the MOB ~20° below the horizontal plane of the Paxinos and Franklin (2001) mouse stereotaxic atlas and along the mediolateral axis by 10–15° to raise the hemisphere being sectioned. This orientation results in a slightly oblique para-horizontal section which retains the rostral portion of the LOT as well as the centrally located CFF tract (see Fig. 1*D*). The resulting slices were placed in a holding chamber that contained artificial cerebrospinal fluid (ACSF) at 30°C, aerated with 95% O_2-5% CO_2. After a 1-h recovery period, the slices were maintained in the same chamber at room temperature. ACSF was composed of (in mM) 124 NaCl, 25 $NaHCO_3$, 5 *N*,*N*-bis[2-hydroxyethyl]-2-aminoethanesulfonic acid (BES), 3 KCl, 1.3 $MgSO_4$, 2.0 $CaCl_2$, and 15 glucose.

Electrical stimulation and field potential recordings

Bipolar stimulation electrodes (paired 50-μm stainless steel wires, insulated except at the tips) were placed in the LOT and/or the CFF tract (Figs. 1*D* and 2*A*). Constant current pulses (20–400 μA, 150 μs) were delivered through an optically isolated stimulus isolator (Grass PSIU6, Quincy, MA) driven by a pulse generator (Grass S48). The pulse generator was also used to trigger image acquisition by the A/D converter (see following text). Glass pipettes (filled with 2 M NaCl, 2–5 MΩ) were placed in the EPL or GCL to record evoked field potentials. Field potential recordings were filtered at 0.1 Hz to 3 kHz, digitized on-line at 20 kHz, and stored on an Apple Macintosh computer.

Imaging VSD signals

Individual slices were stained with the VSD RH-414 (100 μM; Molecular Probes, Eugene, OR). The dye was dissolved in ACSF, and a single slice was placed in a static bath containing this solution, continuously aerated with 95% O_2-5% CO_2 for 30–45 min. The stained slice was then transferred to an immersion-type recording chamber and continuously perfused at 2 ml/min with ACSF at room temperature. Methods used for recording VSD optical signals are similar to those described in detail elsewhere (Keller et al. 1998; Laaris et al. 2000; Wu and

Cohen 1993). To wash out unbound dye, stained slices were perfused with ACSF for ≥15 min before initiating the optical recording. The recording chamber was mounted on a fixed stage upright microscope (BX50WI; Olympus Optical, Tokyo, Japan), rigidly mounted on a vibration-isolation table. A stabilized DC power source was used to power a 100-W tungsten-halogen lamp, and the light from this lamp was band-limited with interference (540 ± 30 nm band-pass; Omega Optical, Brattleboro, VT) and heat filters. Light from the preparation was collected through a ×10 water-immersion objective (0.3 NA, Olympus) and projected onto a hexagonal 464-element array of photodiodes (NeuroPlex, OptImaging, Fairfield, CT). Each photodiode sampled optical signals from a region of ~60 × 60 μm^2. The current output from each photodiode was separately converted to voltages and amplified in two separate stages (×1,000), multiplexed, and digitized at 12-bit resolution with an A/D converter. Optical signals were filtered at 500 Hz before digitizing. All electronic components are part of the commercial NeuroPlex system. Data were collected and stored on a personal computer controlled by NeuroPlex software.

To precisely identify the regions in the slice from which optical recordings were collected, a custom-designed beam splitting device (Microscope Services, Rockville, MD) was used to simultaneously project the images of the slice and light from light-emitting diodes embedded in the photodiode array onto the image plane of a CCD camera (Dage CCD72, Michigan City, IN). This allowed us to demarcate the locations of glomeruli, and of laminar boundaries. These anatomical features, observed in unstained slices, correlated well with their appearance in Nissl-stained sections.

Optical recordings were obtained at a sample rate of 1.63 kHz. Optical responses depicted represent the average of five consecutive traces, collected at 20-s intervals. To correct for spatial differences in illumination intensity and light path length, the signal recorded from each detector was divided by the resting light intensity calculated for the corresponding detector. The resting light intensity for each detector was calculated by subtracting the intensity values recorded while the shutter was closed from those recorded while the shutter was open, when no stimulation was applied. The resulting signal amplitudes are expressed as a fractional change in fluorescence, relative to baseline fluorescence levels ($\Delta F/F_0$). To quantify the relative changes in light fluorescence, we calculated the mean ± SE of the $\Delta F/F_0$ during the 50 ms preceding the stimulus; LOT or CFF poststimulus response amplitudes are expressed as the mean ± SE above these mean baseline values. Analyses of data were performed on an Apple Macintosh computer, using routines developed in Igor (WaveMetrics, Lake Oswego, OR). The peak amplitude and half-width of LOT- and CFF-evoked field potentials and optical signals were calculated from the control and compared with the responses collected after drug application using paired student's *t*-test, and expressed as a percentage of the control. To illustrate the spatial distribution of optical signals (Fig. 3), poststimulus signal amplitudes were color-coded and interpolated as a percentage of the prestimulus signal amplitude.

In addition to VSD-related signals, optical responses may also arise from sources intrinsic to the slice (Grinvald et al. 1988; Yuste et al. 1997). To determine if such intrinsic signals contributed to the waveforms recorded in our study, we performed experiments in slices that were not stained with the VSD ($n = 2$); no optical signals were detected in these control experiments. We also tested the dependence of these signals on the illumination wavelength. When the illumination was changed to a wavelength outside the absorption spectrum of the dye (≥800 nm), no optical signal was detected in the MOB. This suggests that the optical signals represent dye-related responses and are not the result of intrinsic optical signals. Dye-related optical signals may also originate from activation of glial cells. In this case, the optical responses recorded from glial cells are expected to exhibit a slow time course (>1 s) compared with that of neuronal responses (Konnerth et al. 1987). In the mouse MOB, glomerular layer astrocytes exhibit long-lasting (~1 s) responses to single olfactory nerve shocks (De Saint Jan

and Westbrook 2005). However, the evoked optical signals recorded in the present study had only a single depolarizing component, whose duration was <85 ms. Additionally, previous studies demonstrate that glial toxins do not alter VSD optical signals in MOB evoked by olfactory nerve stimulation (Keller et al. 1998). Taken together, these findings suggest that the dye-related optical signals analyzed in the present study reflect neuronal responses and are not related to signals originating from glial cells.

Pharmacological and ionic manipulations

Pharmacological agents were prepared immediately before use from stock solutions and dissolved in ACSF. The following agents were obtained from RBI-Sigma (Natick, MA): D-(–)-2-amino-5-phosphonopentanoic acid (AP5), and tetrodotoxin (TTX). Nominally Ca^{2+}-free solutions were prepared by replacing Ca^{2+} with equimolar concentrations of Mg^{2+}; nominally Mg^{2+}-free solutions were prepared by replacing Mg^{2+} with equimolar concentrations of Ca^{2+}.

RESULTS

Location and segregation of LOT and CFF tracts

The MOB is connected to the frontal pole of the brain by a slender stalk referred to as the olfactory peduncle. Collectively, the olfactory peduncle includes the AON, tenia tecta, and dorsal peduncular cortex (Haberly and Price 1978). The peduncle also contains two major fibers tracts: the LOT, the major output fiber system of the bulb consisting of the axons of mitral/tufted cells, located on the lateral surface of the peduncle, and the anterior commissure, a fiber tract that carries the bulk of centrifugal afferent inputs to the MOB, located at the center of the peduncle (Davis and Macrides 1981); we refer to anterior commissure here as the CFF tract. One goal of the present study was to determine if these two tracts can be independently stimulated in the slice preparation to selectively activate these two major input and output systems of the MOB in electrophysiology experiments. Although the location of the efferent and afferent fiber tracts between MOB and olfactory cortex were described close to a century ago (Cajal 1911), their degree of separation at the caudal pole of the mouse MOB and whether mitral/tufted cell axons and CFFs uniformly segregate into one of the two pathways is unclear.

To verify the distribution of axons in these two fiber tracts, we first placed DiI and DiA crystals into the tracts at the level of the AON in fixed, intact brains. The pattern of labeling was identical in all experiments ($n = 3$ brains). DiI placed into the LOT retrogradely labeled mitral cells in the mitral cell layer (MCL) and tufted cells throughout the EPL as well as lateral/apical dendrites in the EPL and apical dendritic tufts in the GL (Fig. 1, *A* and *C*). The axons of mitral/tufted cells in the bulb coalesced within and projected mainly though the IPL, although many small mitral/tufted cell axon bundles “cut corners” and projected through the superficial granule cell regions en route to the LOT at the caudal aspect of the MOB. DiA placed into the CFF tract labeled a dense plexus of axons and terminals throughout the GCL (Fig. 1, *B* and *C*). Labeled fibers were sparse in the EPL and GL. Tracer injections into the CFF tract never labeled mitral or tufted cells. These results show that the bulk of projections coursing through the CFF tract preferentially terminate in the GCL and IPL.

To confirm the location and axonal distribution of these fiber tracts in the slices used in electrophysiology experiments, we implanted DiI in the CFF tract and DiA in the in LOT in 400-μM-thick quasi-horizontal slices (Fig. 1, *D* and *E*). Because the LOT and CFF tract are located near the floor of the rostral forebrain, only one or two slices through the ventral MOB contained both tracts. Inspection of fresh wet mounts indicates that both tracts are well preserved and separated by 0.8–1.0 mm (Fig. 1*D*). DiI placements into the CFF tract ($n = 4$) anterogradely labeled axons that projected widely throughout the GCL but did not retrogradely

label mitral/tufted cells (Fig. 1*E*). In contrast, DiA labeling of the LOT was highly selective for mitral/tufted cells (Fig. 1*E*).

Origin and time course of LOT- and CFF-evoked responses

LOT STIMULATION—Consistent with previous findings in vivo and in MOB slices (Aroniadou-Anderjaska et al. 1999; Nickell and Shipley 1992; Rall et al. 1966), single LOT shocks (20–100 μA) elicited a negative field potential in the EPL (not shown), reflecting inward currents in the distal dendrites of granule cells and a corresponding positive field potential in the GCL (Fig. 2*B*, Table 1), reflecting outward currents in granule cell somata. LOT-evoked field potentials in the GCL exhibited a single peak at a latency of 7.3 ± 0.8 ms and a duration of 27.9 ± 4.1 ms (n = 10). The GCL field potential did not contain an early presynaptic fiber component. However, LOT-evoked field potentials recorded in the EPL or MCL exhibited an early component in some slices with an onset latency of 1.3 ± 0.2 (n = 7, Table 1); the exact onset latency of the early component could not be measured accurately in all experiments as it sometimes overlapped with the stimulation artifact. This presynaptic component persisted in the presence of glutamate receptor antagonists or Ca^{2+}-free ACSF but was abolished by TTX (data not shown). LOT-evoked optical signals in the GCL (n = 23; Fig. 2, *A* and B, Table 2) had a slower onset latency (10.0 ± 0.6 ms) and a longer duration (66.9 ± 3.8 ms) than the corresponding field potential recorded in the GCL. An early presynaptic component of the optical signal was not detected in the GCL or other MOB layers. This may be due to the organization of mitral cells in a thin layer of neurons, to the relatively low sampling frequency, or to the relatively low numerical aperture of the objective used.

CFF STIMULATION—Consistent with results in vivo (Mori and Takagi 1978; Nakashima et al. 1978; Nickell and Shipley 1993), shocks to the CFF tract produced a negative field potential in the GCL, reflecting inward currents in the proximal dendrites and somata of granule cells (Fig. 2*C*, Table 1) and a corresponding positive field potential in the EPL, reflecting outward currents in granule cell distal dendrites. Typically, CFF stimulation required intensities two- to threefold higher (100–400 μA) than those for LOT stimulation to produce responses of equivalent amplitude. This may due to greater preservation of LOT fibers than CFFs in the slice or to other factors such as the diameter or excitability of the CFFs. The CFF-evoked GCL field potential had two major components: an early negativity (3.5 ± 0.4 ms onset latency, n = 5), followed by a larger-amplitude, longer-duration negativity (8.2 ± 0.4 ms onset latency, 30.8 ± 2.2 ms duration; n = 8). The corresponding optical signal in the GCL had two components (Fig. 2*B*): a fast component (3.0 ± 0.3 ms onset latency, n = 16) apparent in some cases only after application of Ca^{2+}-free ACSF (see following text), followed by a larger-amplitude, slow component (6.8 ± 0.4 ms onset latency, 71.6 ± 3.8 ms duration; n = 27). The early component of the CFF-evoked field potential and optical signal may correspond to a compound action potential in the CFFs, as it was most frequently observed when the GCL recordings were made close to the stimulation site. Consistent with this, the early component of CFF-evoked field potential and optical responses persisted when the slices were perfused with nominally Ca^{2+}-free ACSF to suppress synaptic transmission, whereas the later, slow components were abolished (n = 6; Fig. 2*B*). The early component of CFF-evoked responses that persisted in Ca^{2+}-free ACSF was eliminated by subsequent application of TTX (0.5 μM; n = 6); no responses remained under this condition (Fig. 2*C*). Additionally, the early component was unaffected by glutamate receptor antagonists, whereas the second component was reduced or eliminated (see following text). These findings indicate that the slow component of the field potentials and optical signals elicited by LOT and CFF stimulation reflect postsynaptic depolarization of granule cells mediated by Ca^{2+}-dependent synaptic transmission. By contrast, the early components represent the presynaptic compound action potential in LOT and CFF axons.

Spatial distribution of optical signals

To analyze the spatial distribution of the LOT- and CFF-evoked optical responses in MOB, we generated color-coded maps representing the amplitude of the responses recorded by each photodiode (Fig. 3*A*). In these experiments, we compared patterns of activity elicited by stimulation intensities near-threshold for eliciting optical responses to those elicited by 2×-threshold intensities. LOT stimulation intensities varied from 20 to 60 μA and produced a similar response pattern in all slices ($n = 30$) with small exceptions noted in the following text. As shown in Fig. 3*A*, responses elicited by near-threshold LOT stimulation were first observed in the deep EPL/MCL (7.3 ± 0.4 ms onset latency) and then spread sequentially into the superficial EPL and into the IPL and then the GCL (10.0 ± 0.6 ms onset latency). With near-threshold level LOT stimulation, responses were not observed in the GL. A twofold increase in LOT stimulation intensity increased the amplitude and enlarged the spatial extent of the region from which optical responses were recorded, but the spatiotemporal pattern of evoked responses was similar to that just described for near-threshold stimulation (Fig. 3*A*, Table 2). However, in a subset of slices (7/30) suprathreshold intensity LOT stimulation evoked responses that spread into the GL (8.9 ± 0.6 ms onset latency).

By contrast to LOT stimulation, CFF-evoked responses (200–400 μA) were first observed in the deeper layers and spread sequentially to more superficial layers of MOB (Fig. 3*A*). In all slices, near-threshold intensity CFF shocks elicited responses that were first observed in the deep GCL (6.8 ± 0.5 ms onset latency), then spread progressively into the superficial GCL/IPL and then into to the EPL (10.9 ± 0.8 ms onset latency). There was no spread of the optical signal to the GL. As in the case of LOT stimulation, a doubling of the CFF stimulation intensity increased the amplitude and expanded the region from which optical responses were recorded, but responses remained restricted to the GCL, MCL and EPL, except in rare cases ($n = 4/27$) where the activity spread to the GL (11.7 ± 2.4 ms onset latency).

Glutamate receptors mediate evoked activity

We next investigated the contribution of ionotropic glutamate receptors to the postsynaptic components of field potentials and optical signals evoked by LOT and CFF stimulation. As shown in Fig. 3*B* and Table 3, application of the NMDA receptor antagonist AP5 (100 μM) resulted in a 21.9 ± 1.8% reduction ($n = 5$, $P < 0.004$) in the amplitude, and a small but nonsignificant 11.1 ± 6% reduction ($n = 5$, $P > 0.1$) in the half-width of the LOT-evoked optical signals in the GCL. Similarly, AP5 reduced the amplitude of CFF-evoked optical signal in the GCL by 52.2 ± 8.9% ($n = 5$, $P < 0.05$); the half-width was reduced by 26.3 ± 9.2%, although this trend did not reach statistical significance ($n = 5$, $P > 0.05$). AP5 also reduced the spatial distribution of LOT- and CFF-evoked optical responses (Fig. 3*B*), although this effect was not statistically quantified. By contrast, AP5 did not significantly affect LOT- or CFF-evoked field potentials ($n = 5–6$, $P > 0.05$; see Table 3). Application of CNQX (25 μM; $n = 6$) in the presence of AP5 resulted in complete suppression of the late, postsynaptic components of LOT- and CFF-evoked field potentials and optical signals recorded in all layers (Fig. 3*B*; 95–100% decrease in peak amplitude, $P < 0.05$). Neither AP5 nor CNQX altered the early presynaptic component of the evoked responses (data not shown). Taken together, these findings indicate that in normal physiological conditions, granule cell responses to input from mitral/tufted cells as well as from CFFs are mediated by activation of ionotropic glutamate receptors with dominant AMPA and moderate NMDA receptor-mediated components

Extracellular Mg^{2+} has been shown to limit activation of NMDA receptors on granule cells in response to input from mitral/tufted cells (Aroniadou-Anderjaska et al. 1999; Chen et al. 2000; Isaacson and Strowbridge 1998; Schoppa et al. 1998). We therefore reasoned that enhanced activation of these receptors would increase the magnitude and/or the spatial spread of activity in response to LOT or CFF stimulation. To investigate this, we perfused slices with

a nominally Mg^{2+}-free ACSF (0 Mg^{2+}), a condition that enhances the activation of NMDA receptors (Collingridge and Bliss 1995). Optical signals evoked by near-threshold LOT and CFF stimulation were recorded in normal ACSF and then 5–10 min after perfusion with Mg^{2}–free ACSF. As shown in Fig. 3*C* and Table 3, Mg^{2+}-free ACSF significantly increased (25–43%) the amplitude LOT- and CFF-evoked field potentials and optical signals. The half-width of the signals were also increased (22–29%), although this trend did not reach statistical significance for field potentials (Table 3). Mg^{2+}-free ACSF also appeared to enlarge the spatial extent of LOT- and CFF-evoked optical responses (Fig. 3*C*), although this trend was not statistically analyzed. This suggests that reduction of extracellular Mg^{2+} leads to activation of neuronal elements in previously unresponsive regions. Reduced extracellular Mg^{2+} did not produce spontaneously generated optical signals or other seizure-like activity in the MOB. The enhanced amplitude and propagation of evoked optical signals and field potentials in the presence of 0 Mg^{2+} ACSF were completely reversed by subsequent application of AP5 (100 μM, $n = 4$, $P < 0.05$; data not shown), supporting the conclusion that reduced Mg^{2+} resulted in enhanced activation of NMDA receptors.

DISCUSSION

The results of the present study demonstrate that activation of the LOT and CFF tract elicit complementary activity patterns in mouse MOB slices. LOT-evoked responses initiate in the MCL/EPL and propagate into the deeper layers, whereas CFF-evoked responses appear first in the deep GCL and propagate more superficially. Both patterns reflect excitatory postsynaptic activity in granule cells involving AMPA and NMDA receptor-mediated components. Stimulation of the LOT and CFF tracts can be used, respectively, to selectively activate anatomically segregated excitatory inputs to the distal versus proximal dendrites/somata of granule cells in MOB slice preparations.

Location and distribution of LOT and CFF axons

The present tract tracing results show that tracer deposits into the CFF tract in vivo or in vitro produced dense anterograde labeling that was concentrated in the deep part of the GCL. Moderate labeling was present in the superficial GCL and the IPL; sparser labeling was present in the EPL whereas the GL was nearly devoid of labeled fibers. This pattern of labeling is consistent with the distribution of afferent fibers from several olfactory cortical areas [piriform cortex, periamygdaloid nucleus, nucleus of the LOT, AON (pars dorsalis, medial and ventroposterior)] previously reported to terminate heavily in the GCL but only sparsely in the GL (Luskin and Price 1983; Pinching and Powell 1972). More superficial layers of the MOB (i.e., the EPL and GL) receive dense inputs from some divisions of AON (pars medialis and ventroposterior) (Luskin and Price 1983) as well as from cholinergic and serotonergic cell groups (for review, see Ennis et al. 2006). The relatively sparse labeling in the superficial layers in the present study suggests that those fibers terminating superficially in MOB course through other regions of the olfactory peduncle than targeted by our tracer injections. Consistent with this, afferent fibers terminating in the EPL and GL (e.g., from AON pars medialis and serotonergic nuclei) bypass the CFF tract and course through the medial aspect of the olfactory peduncle to enter MOB (Davis and Macrides 1981; McLean and Shipley 1987). Cholinergic, noradrenergic, and GABAergic fibers enter the MOB via the medial forebrain bundle located ventral to the CFF tract (Fallon and Moore 1978; Macrides et al. 1981; McLean et al. 1989). Additionally, the present findings demonstrate that CFF stimulation did not produce discernible field potential or VSD-optical responses in the presence of ionotropic glutamate receptor antagonists, indicating a minimal contribution from noradrenergic, serotonergic, or cholinergic fibers. However, we cannot exclude the possibility that release of neurotransmitter from these inputs modulated the intensity or time course of the responses evoked in normal ACSF.

Origin of LOT- and CFF-evoked signals

The results of this study indicate that the longer-latency components of LOT- and CFF-evoked responses primarily reflect postsynaptic activity in MOB neurons. Consistent with this, the longer-latency components of the evoked responses were abolished when the slice was perfused with zero-Ca^{2+} ACSF or with ionotropic glutamate receptor antagonists (CNQX + AP5). The later finding indicates that the initiation of postsynaptic activity requires activation of ionotropic glutamate receptors.

The laminar profiles and opposite polarity of LOT- and CFF-evoked field potentials in the EPL and GCL are entirely consistent with previous findings in vivo and in vitro that these potentials reflect postsynaptic responses generated by transmembrane current flow through the granule cell dipole (Aroniadou-Anderjaska et al. 1999; Martinez and Freeman 1984; Mori and Takagi 1978; Nakashima et al. 1978; Neville and Haberly 2003; Nickell and Shipley 1992, 1993; Patneau and Stripling 1992; Rall et al. 1966; Stripling et al. 1991). The spatiotemporal pattern of VSD optical responses in the different layers of the bulb is also consistent with this conclusion. Thus LOT-evoked responses were first observed in the MCL/EPL and subsequently in the GCL or the GL. Responses in the MCL may reflect activation of superficial granule cells in this layer as the MCL contains ~100,000 superficially located granule cells (Frazier and Brunjes 1988) compared with ~40,000 mitral cells (Meisami 1989). CFF-evoked responses, by contrast, were always observed first in the GCL and subsequently in more superficial layers. Taken together, these findings indicate that within the range of stimulation currents used (20–400 μA), the LOT and CFF tracts can be independently activated in rodent MOB slices and used to selectively activate anatomically segregated inputs to the distal dendrites versus proximal dendrites/somata of granule cells.

One possible exception to this conclusion is the observation of evoked optical signals in the GL in a small subset of slices. Granule cell processes do not enter the GL (Cajal 1911; Ennis et al. 2006). The layers of the MOB are organized as concentric circles. Because of this curvature in 400-μm-thick slices, the laminar borders are imprecise as neural elements in one layer may be superimposed above or below an adjacent layer; i.e., a parallax error. Thus the evoked optical signals observed in the GL may represent activity in granule cell dendrites in the superficial EPL.

Optical signals primarily reflect membrane potential changes and unlike field potentials would include contributions from neurons that do not from dipoles. Thus LOT-evoked optical signals may reflect depolarization of other neuron types that receive input from mitral/tufted cells, including periglomerular/short axon cells in the GL, intrinsic interneurons in the EPL, granule cells in the MCL, and nongranule interneurons in the GCL (Ennis et al. 2006). Similarly, the CFF-evoked optical signal may reflect contributions from nongranule cell neurons targeted by CFFs in the GCL and EPL. However, the amplitude of the optical signal is directly proportional to the surface area of the membranes from which the signal is recorded (assuming uniform dye binding) (Grinvald et al. 1988; Salzberg et al. 1973). Although we do not exclude contributions from other cell types, because granule cell somata and dendrites are the most numerous neuronal elements in the EPL and GCL postsynaptic to mitral/tufted cells (via LOT stimulation) or CFF inputs, most of the optically recorded responses in these layers should originate from granule cells.

An additional consideration is the possibility that LOT-evoked activity reflects mitral/tufted cell excitation elicited by glutamate spillover among the apical or lateral dendrites of these cells. Several findings indicate that the contribution of mitral/tufted cell glutamate spillover is minor. First, mitral cell self-excitation in normal ACSF is negligible or absent. In physiological conditions in MOB slices, spikes in mitral cells are followed by IPSPs, and postspike glutamatergic excitation can only be observed when extracellular Mg^{2+} is eliminated or when

$GABA_A$ receptors are blocked (Friedman and Strowbridge 2000; Isaacson 1999; Salin et al. 2001). Other studies performed in normal media have reported that antidromic activation of a population of mitral cells, or in some cases single spikes in one mitral cell, elicit spillover-mediated lateral excitation of other mitral cell apical dendrites which extend into the same glomerulus (Carlson et al. 2000; Christie et al. 2005; Schoppa and Westbrook 2002; Urban and Sakmann 2002). The glomerulus specific spillover-mediated excitation was of short latency (1–2 ms flowing somatic spike) (Schoppa and Westbrook 2002; Urban and Sakmann 2002) or of very long duration (≥1 s) (Carlson et al. 2000). In the present study, LOT-evoked optical signals in the glomerulus were of longer latency (>6 ms after presynaptic spike in the MCL) and of shorter duration (<85 ms) than spillover-mediated responses. These findings suggest that that the LOT-evoked optical responses in the GL in present study reflect responses in granule cell dendrites and/or depolarization of periglomerular or short axon glomerular neurons. CFF stimulation is unlikely to cause glutamate spillover as it produces IPSPs in mitral cells after the initial activation of granule cells (Mori and Takagi 1978; Nicoll 1971; Yamamoto et al. 1963).

Pre- and postsynaptic components of evoked signals

The LOT-evoked field potential recorded in the MCL/EPL contained an early component corresponding to the presynaptic compound action potential in mitral/tufted cells as it persisted in antagonists of ionotropic glutamate receptors or Ca^{2+}-free ACSF but was abolished by the Na^+ channel blocker TTX. Assuming a straight line distance between the stimulation and recording sites of ~2.2 mm, the latency of the presynaptic spike (1.3 ms) translates to a LOT axon impulse conduction velocity of 1.7 m/s. However, this value probably underestimates the conduction velocity as the onset of the presynaptic component could not be measured in some experiments due to overlap with the stimulation artifact. This may account for the slower conduction velocity of LOT axons in the present study compared with that reported for juvenile (P15) rats, 2.7 m/s (Schwob et al. 1984). Similar calculations for the presynaptic component observed in CFF-evoked field potentials (3.5 ms) and optical signals (3.0 ms), assuming a 2.0 mm straight line distance between stimulation and recording sites, yield CFF axonal conduction velocities of 0.5 and 0.6 m/s, respectively. These values are comparable to the 0.4 m/s impulse conduction velocity of AON and piriform cortex CFFs reported in adult rats (Moyano and Molina 1980).

Based on the relative latencies of the postsynaptic component of evoked optical signal across different layers of MOB, LOT-evoked signals spread from the EPL into the GCL or the GL with an estimated conduction velocity of 0.2 m/s. CFF-evoked optical signals spread from the GCL to the more superficial layers with an estimated conduction velocity of 0.2 m/s. The values for the interlaminar spread of optical signals are substantially lower than the respective conduction velocities of LOT axons and CFFs in this study (see preceding text). The similar interlaminar postsynaptic conduction velocity for LOT- and CFF-evoked optical signals provides additional support that they originate from a common postsynaptic neural element, specifically granule cells. The similar propagation speed for LOT- and CFF-evoked optical responses across the MOB layers suggests that their spatial spread is generated primarily by intrinsic propagation of membrane potential changes along the granule cell following the initial synaptic input as apposed to the temporal delay, for example, in pre-synaptic spikes in CFFs synapsing on deep versus superficial portions of the granule cell.

VSD optical signals primarily reflect changes in membrane potential and thus may include components related to decremental postsynaptic potentials as well as actively propagating Na^+ or Ca^{2+} spikes. Granule cells exhibit somatic and dendritic Na^+ and Ca^{2+} spikes (Egger et al. 2005; Halabisky et al. 2000; Pinato and Midtgaard 2003, 2005; Zelles et al. 2006), but their conduction velocity has not been reported. It is noteworthy that the interlaminar

conduction velocity calculated here for LOT- and CFF-evoked optical signals (0.2 m/s) is similar to the somatofugal spike conduction velocity in mitral cell lateral dendrites (0.20–0.35 m/s) (Djurisic et al. 2004; Xiong and Chen 2002). Further studies are needed to determine the relative contribution of passive and active membrane properties to LOT- and CFF-evoked postsynaptic responses in granule cells.

Role of ionotropic glutamate receptors

LOT- and CFF-evoked field potentials were minimally affected by NMDA receptor blockade, whereas the corresponding evoked optical signals exhibited more substantial reductions. The lack of effect of NMDA receptor blockade on the evoked field potentials may be due to their small amplitude (<0.5 mV) in the submerged slices used in the present study or because the NMDA receptor-mediated response is not in phase across the population of neurons contributing to the field potential. This is less problematic with the VSD signals as they measure membrane potential changes at a discrete spatial location. The weak effect of NMDA receptor blockade observed here is consistent with observations in vivo that the amplitude of LOT-evoked field potential is unaffected by AP5, whereas the duration is slightly reduced (Yokoi et al. 1995). The reduction of the peak amplitude of the LOT-evoked optical signal after NMDA receptor antagonism is consistent with similar reductions of mitral/tufted cell-evoked EPSPs in granule cells in the presence of physiological levels of extracellular Mg^{2+} (Schoppa and Westbrook 1999; Schoppa et al. 1998). This finding is also in agreement with AP5's reduction of VSD-optical signals elicited after antidromic activation of mitral/tufted cells in the salamander olfactory bulb (Wellis and Kauer 1993).

NMDA receptor blockade also markedly attenuated (~50% reduction) the amplitude of the CFF-evoked optical signal, indicating that glutamatergic inputs to granule cell somata and proximal dendrites are mediated by both NMDA and AMPA receptors. The more substantial effects of AP5 on CFF-evoked responses may reflect a greater contribution of NMDA receptors to synaptic inputs to the somata/proximal dendrites of granule cells. LOT- and CFF-evoked field potentials and optical signals were completely blocked in the presence of CNQX and AP5 in agreement with previous studies (Chen et al. 2000; Isaacson 2001; Isaacson and Strowbridge 1998). The enhancement of the amplitude, duration, and spatial extent of LOT-evoked field potentials and optical signals in Mg^{2+}-free ACSF is consistent with previous reports of increased granule cell responses to mitral/tufted cell input and augmented dendrodendritic inhibition of mitral cells in low Mg^{2+} (Chen et al. 2000; Isaacson and Strowbridge 1998; Schoppa et al. 1998; Wellis and Kauer 1993).

Functional considerations

The role of centrifugal projections from olfactory cortical areas to the MOB in olfactory processing is poorly understood. Activation of these inputs was reported to suppress odor-evoked field potential activity in MOB (Kerr and Hagbarth 1955). By contrast, elimination of CFF inputs has been reported to increase odorant receptive fields of MOB neurons and to disrupt synchrony of neuronal discharge with the respiratory cycle (Chaput 1983). More recent work demonstrates that projections from piriform cortex a play a key role in the generation of beta frequency oscillations in MOB. Interestingly, olfactory experience modifies the expression of beta oscillations in MOB. Beta oscillations are enhanced during olfactory learning tasks or repetitive presentations of an odorant (Gray and Skinner 1988; Martin et al. 2004; Ravel et al. 2003). Disruption of cortical centrifugal projections abolishes odor-evoked beta oscillations in MOB and prevent their experience-dependent enhancement (Martin et al. 2006; Neville and Haberly 2003). Lesions of the CFF tract have also been reported to interfere with odor-reward association learning (Kiselycnyk et al. 2006). Other findings demonstrate that olfactory processing in neonatal and mature animals exhibits considerable plasticity as a result of previous odor experience including: alterations in odor-induced activity maps

(Coppersmith and Leon 1986; Johnson and Leon 1996; Montag-Sallaz and Buonviso 2002; Salcedo et al. 2005; Yuan et al. 2002), mitral cell odorant tuning or responsiveness (Buonviso and Chaput 2000; Fletcher and Wilson 2003; Wilson and Leon 1988), and enhanced odorant discrimination (Mandorian et al. 2006a,b). Consistent with the studies cited in the preceding text, such plasticity is likely to involve centrifugal projections to MOB, including those from olfactory cortical areas.

Previous studies suggest that high-frequency stimulation of CFFs produces long-lasting changes in the excitability of MOB neurons. In a fish, CFF stimulation was reported to enhance the development of long-term potentiation (LTP) at mitral cell-togranule cell synapses (Satou et al. 2005). High-frequency stimulation of the GCL in rats has been reported to produce LTP of CFF input to granule cells in vivo (Patneau and Stripling 1992; Stripling et al. 1991). Stimulation of the CFF tract in the slice preparation used in the present study will allow more direct cellular electrophysiological analyses of LTP at mammalian CFF-to-granule cell synapses as well as how activation of these synapses impact on mitral cell-granule cell dendrodendritic interactions. The present slice preparation can also be used to explore the physiological influence of CFF projections on other deep inhibitory interneurons in MOB, including Blanes cells. Recent studies in vitro demonstrate that stimuli that evoked persistent firing in Blanes cells also produced prolonged barrages of inhibitory postsynaptic currents in granule cells (Pressler and Strowbridge 2006). These findings indicate that Blanes cells play a major role in modulating of the excitability state of granule cells, which in turn, may impact on the activity of mitral/tufted output neurons. Inputs from Blanes cells appear to preferentially target the basal dendrites and somata of granule cells. If Blanes cells are targeted by CFF inputs, then the direct activation of granule cells by centrifugal cortical inputs may be followed by a prolonged epoch of granule cell inhibition via the Blanes cells. Thus the activity state of Blanes cells may provide a critical gate on excitatory feedback projections from olfactory cortical structures to granule cells, perhaps allowing granule cell-mitral cell dendrodendritic synapses to operate independently of inputs to granule cell basal dendrites/somata.

Acknowledgments

This work was supported in part by National Institute on Deafness and Other Communication Disorders Grants DC-03195 and DC-00347.

REFERENCES

Aroniadou-Anderjaska V, Ennis M, Shipley MT. Current-source density analysis in the rat olfactory bulb: laminar distribution of kainate/AMPA and NMDA receptor-mediated currents. J Neurophysiol 1999;81:15–28. [PubMed: 9914263]

Buonviso N, Chaput M. Olfactory experience decreases responsiveness of the olfactory bulb in the adult rat. Neuroscience 2000;95:325–32. [PubMed: 10658611]

Cajal, RSY. Histologie du Systeme Nerveux de l'Hommes et des Vertebres. Maloine; Paris: 1911.

Carlson GC, Shipley MT, Keller A. Long-lasting depolarizations in mitral cells of the rat olfactory bulb. J Neurosci 2000;20:2011–21. [PubMed: 10684902]

Chaput M. Effects of olfactory peduncle sectioning on the single unit responses of olfactory bulb neurons to odor presentation in awake rabbits. Chem Senses 1983;8:161–177.

Chen WR, Xiong W, Shepherd GM. Analysis of relations between NMDA receptors and GABA release at olfactory bulb reciprocal synapses. Neuron 2000;25:625–633. [PubMed: 10774730]

Christie JM, Bark C, Hormuzdi SG, Helbig I, Monyer H, Westbrook GL. Connexin36 mediates spike synchrony in olfactory bulb glomeruli. Neuron 2005;46:761–772. [PubMed: 15924862]

Collinridge GL, Bliss TVP. Memories of NMDA receptors and LTP. Trends Neurosci 1995;18:54–56. [PubMed: 7537406]

Coopersmith R, Leon M. Enhanced neural response by adult rats to odors experienced early in life. Brain Res 1986;371:400–403. [PubMed: 3697770]

Davis BJ, Macrides F. The organization of centrifugal projections from the anterior olfactory nucleus, ventral hippocampal rudiment, and piriform cortex to the main olfactory bulb in the hamster: an autoradiographic study. J Comp Neurol 1981;203:475–493. [PubMed: 6274922]

De Saint Jan D, Westbrook GL. Detecting activity in olfactory bulb glomeruli with astrocyte recording. J Neurosci 2005;25:2917–2924. [PubMed: 15772351]

Djurisic M, Antic S, Chen WR, Zecevic D. Voltage imaging from dendrites of mitral cells: EPSP attenuation and spike trigger zones. J Neurosci 2004;24:6703–6714. [PubMed: 15282273]

Egger V, Svoboda K, Mainen ZF. Dendrodendritic synaptic signals in olfactory bulb granule cells: local spine boost and global low-threshold spike. J Neurosci 2005;25:3521–3530. [PubMed: 15814782]

Ennis, M.; Hamilton, KA.; Hayar, A. Neurochemistry of the main olfactory system.. In: Lajtha, A., editor. Handbook of Neurochemistry and Molecular Neurobiology. Vol. 3rd ed.. Springer; New York: In press

Fallon JH, Moore RY. Catecholamine innervation of the basal forebrain. III. Olfactory bulb, anterior olfactory nuclei, olfactory tubercle and piriform cortex. J Comp Neurol 1978;180:533–554. [PubMed: 307009]

Fletcher ML, Wilson DA. Olfactory bulb mitral-tufted cell plasticity: odorant-specific tuning reflects previous odorant exposure. J Neurosci 2003;23:6946–6955. [PubMed: 12890789]

Frazier LL, Brunjes PC. Unilateral odor deprivation: early postnatal changes in olfactory bulb cell density and number. J Comp Neurol 1988;269:355–370. [PubMed: 3372719]

Friedman D, Strowbridge BW. Functional role of NMDA autoreceptors in olfactory mitral cells. J Neurophysiol 2000;84:39–50. [PubMed: 10899181]

Gray CM, Skinner JE. Centrifugal regulation of olfactory bulb of the waking rabbit as revealed by reversible cryogenic blockade. Exp Brain Res 1988;69:378–386. [PubMed: 3345814]

Grinvald A, Frostig RD, Lieke E, Hildesheim R. Optical imaging of neuronal activity. Physiol Rev 1988;68:1285–1366. [PubMed: 3054949]

Haberly LB, Price JL. Association and commissural fiber systems of the olfactory cortex of the rat. I. Systems originating in the piriform cortex and adjacent areas. J Comp Neurol 1978;178:711–740. [PubMed: 632378]

Halabisky B, Friedman D, Radojicic M, Strowbridge BW. Calcium influx through NMDA receptors directly evokes GABA release in olfactory bulb granule cells. J Neurosci 2000;20:5124–34. [PubMed: 10864969]

Heinbockel T, Heyward PM, Ennis M. Potent regulation of main olfactory bulb mitral cell excitability by metabotropic glutamate receptor mGluR1. J Neurophysiol 2004;92:3085–3096. [PubMed: 15212418]

Isaacson JS. Glutamate spillover mediates excitatory transmission in the rat olfactory bulb. Neuron 1999;23:377–384. [PubMed: 10399942]

Isaacson JS. Mechanisms governing dendritic gamma-aminobutyric acid (GABA) release in the rat olfactory bulb. Proc Natl Acad Sci 2001;98:337–342. [PubMed: 11120892]

Isaacson JS, Strowbridge BW. Olfactory reciprocal synapses: dendritic signaling in the CNS. Neuron 1998;20:749–761. [PubMed: 9581766]

Johnson BA, Leon M. Spatial distribution of [^{14}C]2-deoxyglucose uptake in the glomerular layer of the rat olfactory bulb following early odor preference learning. J Comp Neurol 1996;376:557–566. [PubMed: 8978470]

Keller A, Yagodin S, Aroniadou-Anderjaska A, Zimmer LA, Ennis M, Sheppard NF, Shipley MT. Functional organization of rat olfactory bulb glomeruli revealed by optical imaging. J Neurosci 1998;18:2602–2612. [PubMed: 9502819]

Kerr DIB, Hagbarth KE. An investigation of the olfactory centrifugal system. J Neurophysiol 1955;18:362–374. [PubMed: 13243143]

Kiselycznyk CL, Zhang S, Linster C. Role of centrifugal projections to the olfactory bulb in olfactory processing. Learn Mem 2006;13:575–579. [PubMed: 16980549]

Konnerth A, Obaid AL, Salzberg DM. Optical recording of electrical activity from parallel fibers and other cell types in skate cerebellar slices in vitro. J Physiol 1987;393:681–702. [PubMed: 3446807]

Laaris N, Carlson GC, Keller A. Thalamic-evoked synaptic interactions in barrel cortex revealed by optical imaging. J Neurosci 2000;20:1529–1537. [PubMed: 10662842]

Luo M, Katz LC. Response correlation maps of neurons in the mammalian olfactory bulb. Neuron 2001;32:1165–1179. [PubMed: 11754845]

Luskin MB, Price JL. The topographic organization of associational fibers of the olfactory system in the rat, including centrifugal fibers to the olfactory bulb. J Comp Neurol 1983;216:264–291. [PubMed: 6306065]

Macrides F, Davis BJ, Youngs WM, Nadi NS, Margolis FL. Cholinergic and catecholaminergic afferents to the olfactory bulb in the hamster: a neuroanatomical, biochemical, and histochemical investigation. J Comp Neurol 1981;203:495–514. [PubMed: 6274923]

Mandairon N, Stack C, Kiselycznyk C, Linster C. Broad activation of the olfactory bulb produces long-lasting changes in odor perception. Proc Natl Acad Sci USA 2006a;101:13543–13548.

Mandairon N, Stack C, Kiselycznyk C, Linster C. Enrichment to odors improves olfactory discrimination in adult rats. Behav Neurosci 2006b;120:173–179. [PubMed: 16492127]

Martin C, Gervais R, Hugues E, Messaoudi B, Ravel N. Learning modulation of odor-induced oscillatory responses in the rat olfactory bulb: a correlate of odor recognition? J Neurosci 2004;24:389–397. [PubMed: 14724237]

Martin C, Gervais R, Messaoudi B, Ravel N. Learning-induced oscillatory activities correlated to odour recognition: a network activity. Eur J Neurosci 2006;23:1801–1810. [PubMed: 16623837]

Martinez DP, Freeman WJ. Periglomerular cell action on mitral cells in olfactory bulb shown by current source density analysis. Brain Res 1984;308:223–233. [PubMed: 6478206]

McLean JH, Shipley MT. Serotonergic afferents to the rat olfactory bulb. I. Origins and laminar specificity of serotonergic inputs in the adult rat. J Neurosci 1987;7:3016–3028. [PubMed: 2822862]

McLean JH, Shipley MT, Nickell WT, Aston-Jones G, Reyher CK. Chemoanatomical organization of the noradrenergic input from locus coeruleus to the olfactory bulb of the adult rat. J Comp Neurol 1989;285:339–349. [PubMed: 2547851]

Meisami E. A proposed relationship between increases in the number of olfactory receptor neurons, convergence ratio and sensitivity in the developing rat. Brain Res Dev Brain Res 1989;46:9–19.

Montag-Sallaz M, Buonviso N. Altered odor-induced expression of c-fos and arg 3.1 immediate early genes in the olfactory system after familiarization with an odor. J Neurobiol 2002;52:61–72. [PubMed: 12115894]

Mori K, Takagi SF. Activation and inhibition of olfactory bulb neurones by anterior commissure volleys in the rabbit. J Physiol 1978;279:589–604. [PubMed: 671364]

Moyano HF, Molina JC. Axonal projections and conduction properties of olfactory peduncle neurons in the rat. Exp Brain Res 1980;39:241–248. [PubMed: 7398820]

Nakashima M, Mori K, Takagi SF. Centrifugal influence on olfactory bulb activity in the rabbit. Brain Res 1978;154:301–316. [PubMed: 687996]

Neville KR, Haberly LB. Beta and gamma oscillations in the olfactory system of the urethan-anesthetized rat. J Neurophysiol 2003;90:3921–3930. [PubMed: 12917385]

Nickell, WT.; Shipley, MT. Neurophysiology of the Olfactory Bulb.. In: Serby, MJ.; Chobor, KL., editors. Science of Olfaction. Springer-Verlag; New York: 1992. p. 172-212.

Nickell WT, Shipley MT. Evidence for presynaptic inhibition of the olfactory commissural pathway by cholinergic agonists and stimulation of the nucleus of the diagonal band. J Neurosci 1993;13:650–659. [PubMed: 8426231]

Nicoll RA. Pharmacological evidence for GABA as the transmitter in granule cell inhibition in the olfactory bulb. Brain Res 1971;35:137–149. [PubMed: 4332422]

Patneau DK, Stripling JS. Functional correlates of selective long-term potentiation in the olfactory cortex and olfactory bulb. Brain Res 1992;585:219–228. [PubMed: 1511305]

Paxinos, G.; Franklin, KBJ. The Mouse Brain in Stereotaxic Coordinates. Vol. 2nd ed.. Academic; San Diego, CA: 2001.

Pinato G, Midtgaard J. Regulation of granule cell excitability by a low-threshold calcium spike in turtle olfactory bulb. J Neurophysiol 2003;90:3341–3351. [PubMed: 12867531]

Pinato G, Midtgaard J. Dendritic sodium spikelets and low-threshold calcium spikes in turtle olfactory bulb granule cells. J Neurophysiol 2005;93:1285–1294. [PubMed: 15483062]

Pinching AJ, Powell TPS. The termination of centrifugal fibres in the glomerular layer of the olfactory bulb. J Cell Sci 1972;10:621–635. [PubMed: 5038408]

Pressler RT, Strowbridge BW. Blanes cells mediate persistent feedforward inhibition onto granule cells in the olfactory bulb. Neuron 2006;49:889–904. [PubMed: 16543136]

Price JL, Powell TPS. An electron-microscopic study of the termination of the afferent fibres to the olfactory bulb from the cerebral hemisphere. J Cell Sci 1970;7:157–187. [PubMed: 5476854]

Rall W, Shepherd GM, Reese TS, Brightman MW. Dendrodendritic synaptic pathway for inhibition in the olfactory bulb. Exp Neurol 1966;14:44–56. [PubMed: 5900523]

Ravel N, Chabaud P, Martin C, Hugues E, Tallon-Baudry, Bertand O, Gervais R. Olfactory learning modifies the expression of odour-induced oscillatory responses in the gamma (60–90 Hz) and beta (15–40 Hz) bands in the rat olfactory bulb. Eur J Neurosci 2003;17:350–358. [PubMed: 12542672]

Salcedo E, Zhang C, Kronberg E, Restrepo D. Analysis of training-induced changes in ethyl acetate odor maps using a new computational tool to map the glomerular layer of the olfactory bulb. Chem Senses 2005;30:615–626. [PubMed: 16141292]

Salin PA, Lledo PM, Vincent JD, Charpak S. Dendritic glutamate autoreceptors modulate signal processing in rat mitral cells. J Neurophysiol 2001;85:1275–1282. [PubMed: 11247996]

Salzberg BM, Davila HV, Cohen LB. Optical recording of impulses in individual neurons of an invertebrate central nervous system. Nature 1973;246:508–509. [PubMed: 4357630]

Satou M, Anzai S, Huruno M. Long-term potentiation and olfactory memory formation in the carp (*Cyprinus carpio* L.) olfactory bulb. J Comp Physiol 2005;191:421–434. [PubMed: 15750817]

Schoppa NE, Kinzie JM, Sahara Y, Segerson TP, Westbrook GL. Dendrodendritic inhibition in the olfactory bulb is driven by NMDA receptors. J Neurosci 1998;18:6790–6802. [PubMed: 9712650]

Schoppa NE, Westbrook GL. Regulation of synaptic timing in the olfactory bulb by an A-type potassium current. Nat Neurosci 1999;2:1106–1113. [PubMed: 10570488]

Schoppa NE, Westbrook GL. AMPA receptors drive correlated spiking in olfactory bulb glomeruli. Nat Neurosci 2002;5:1194–1202. [PubMed: 12379859]

Schwob JE, Haberly LB, Price JP. The development of physiological responses of the piriform cortex in rats to stimulation of the lateral olfactory tract. J Comp Neurol 1984;223:223–237. [PubMed: 6707249]

Stripling JS, Patneau DK, Gramlich CA. Characterization and anatomical distribution of selective long-term potentiation in the olfactory forebrain. Brain Res 1991;542:107–122. [PubMed: 2054649]

Urban NN, Sakmann B. Reciprocal intraglomerular excitation and intra- and interglomerular lateral inhibition between mouse olfactory bulb mitral cells. J Physiol 2002;542:355–367. [PubMed: 12122137]

Wellis DP, Kauer JS. GABAA and glutamate receptor involvement in dendrodendritic synaptic interactions from salamander olfactory bulb. J Physiol 1993;469:315–339. [PubMed: 7903696]

Wilson DA, Leon M. Spatial patterns of olfactory bulb single-unit responses to learned olfactory cues in young rats. J Neurophysiol 1988;59:1770–1782. [PubMed: 3404204]

Wu, J-Y.; Cohen, LB. Fast multisite optical measurement of membrane potential.. In: Mason, WT., editor. Fluorescent and Luminescent Probes for Biological Activity. Academic; London: 1993. p. 389-404.

Xiong W, Chen WR. Dynamic gating of spike propagation in the mitral cell lateral dendrites. Neuron 2002;34:115–126. [PubMed: 11931746]

Yamamoto C, Yamamoto T, Iwama K. The inhibitory systems in the olfactory bulb studied by intracellular recording. J Neurophysiol 1963;26:403–415. [PubMed: 14002306]

Yokoi M, Mori K, Nakanishi S. refinement of odor molecule tuning by dendrodendritic synaptic inhibition in the olfactory bulb. Proc Natl Acad Sci USA 1995;92:3371–3375. [PubMed: 7724568]

Yuan Q, Harley CW, McLean JH, Knopfel T. Optical imaging of odor preference memory in the rat olfactory bulb. J Neurophysiol 2002;87:3156–3159. [PubMed: 12037216]

Yuste R, Tank DW, Kleinfeld D. Functional study of the rat cortical microcircuitry with voltage-sensitive dye imaging of neocortical slices. Cereb Cortex 1997;7:546–558. [PubMed: 9276179]

Zelles T, Boyd JD, Hardy AB, Delaney KR. Branch-specific Ca^{2+} influx from Na^{+}-dependent dendritic spikes in olfactory granule cells. J Neurosci 2006;26:30–40. [PubMed: 16399670]

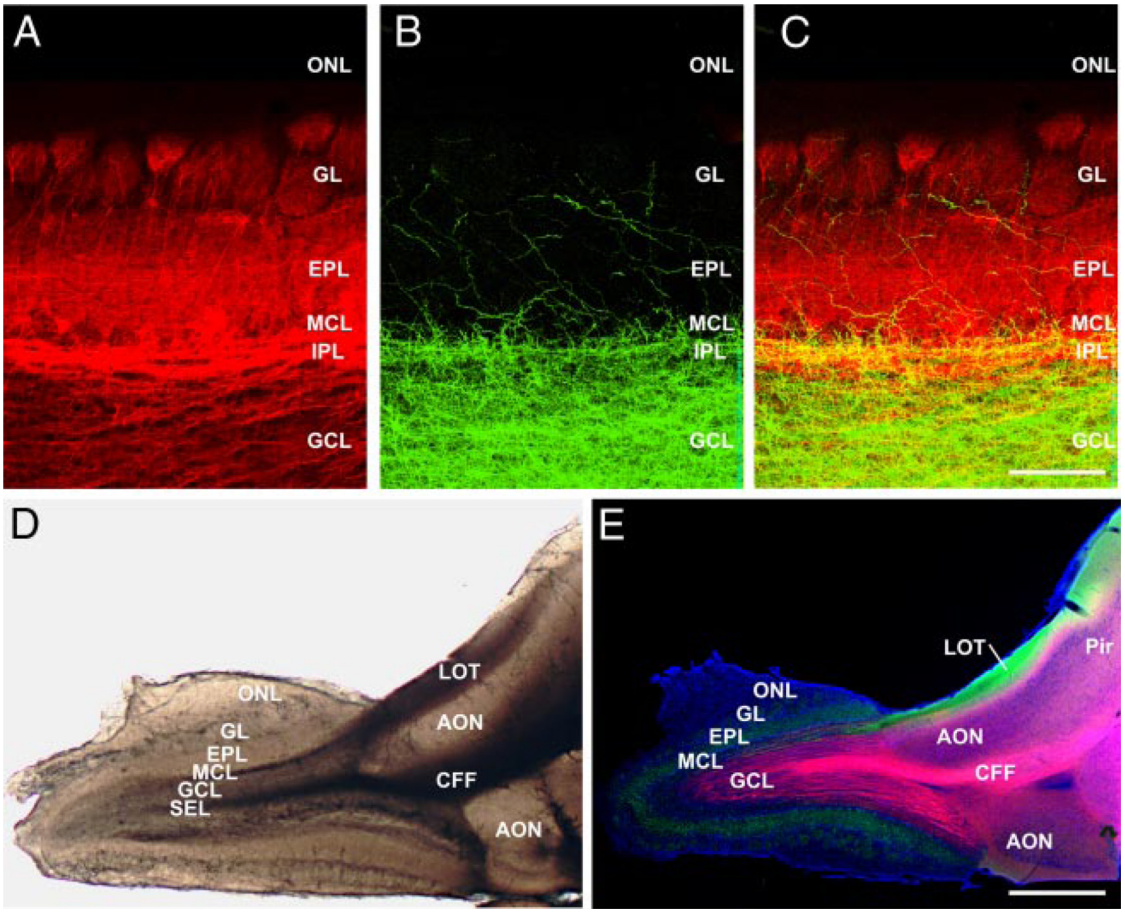

FIG. 1.

Wet mount and tract tracing. *A–C*: labeling in main olfactory bulb (MOB) after dye injections in vivo. *A*: retrograde labeling after DiI placement in the lateral olfactory tract (LOT). Mitral/tufted cell axons, soma and dendrites are heavily labeled. *B*: same section as in *A* showing anterograde labeling after DiA placement in the centrifugal fiber (CFF) tract. The labeled axons terminate heavily in the granule cell and internal plexiform layers, and more sparsely in the superficial layers. C: overlay image of *A* and *B* showing the laminar segregation of labeled fibers and cell bodies. *D*: wet mount preparation of a 400-μm-thick quasi-horizontal forebrain-MOB slice. The LOT and CFF tract are clearly visible at the level of the anterior olfactory nucleus, just caudal to the MOB. Lateral is at the top, rostral to the left. *E*: similar slice as in *D*, in which DiI was placed in the CFF tract and DiA in the LOT; DAPI counterstaining (blue). CFFs (pink staining) project densely into the central bulb while retrograde labeling from the LOT (green staining) distributes through the mitral, external plexiform and glomerular layers. Scale bar = 200 μm in *A–C* and 1 mm in *D* and *E*. AON, anterior olfactory nucleus; EPL, external plexiform layer; GCL, granule cell layer; GL, glomerular layer; IPL, internal plexiform layer; MCL, mitral cell layer; ONL, olfactory nerve layer; Pir, piriform cortex; SEL, subependymal layer.

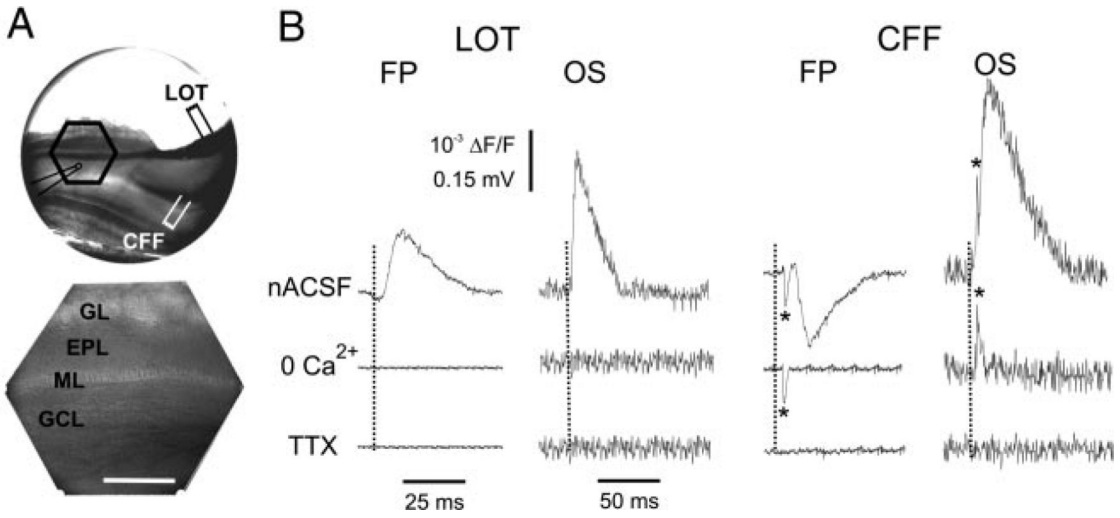

FIG. 2.

LOT- and CFF-evoked field potentials and optical signals. *A*: optical recording setup. *Top*: videographic image of a 400-μm-thick forebrain-MOB slice. Hexagonal frame demarcates the border of the 464-element photodiode array. The position of the field potential electrode, and the CFF and LOT stimulation electrodes are indicated. *Bottom*: higher magnification videographic image of the area within the hexagon in upper panel. Scale bar = 400 μm. *B*, *right* and *left*: simultaneous recordings of field potentials (FPs) and voltage-sensitive dye (VSD) optical signals (OS) in the granule cell layer evoked by LOT (*left*) and CFF (*right*) stimulation (LOT, 20 μA; CFF, 100 μA). In normal artificial cerebrospinal fluid (nACSF, *top traces*), the LOT-evoked FP is positive, whereas the CFF-evoked FP is negative. ⋯, stimulation onset. *, early presynaptic component of the CFF-evoked FP and OS. Note that Ca^{2+}-free ACSF (0 Ca^{2+}, *middle traces*) eliminates all responses except for the early presynaptic component. The presynaptic component is abolished by TTX (0.5 μM, *bottom traces*).

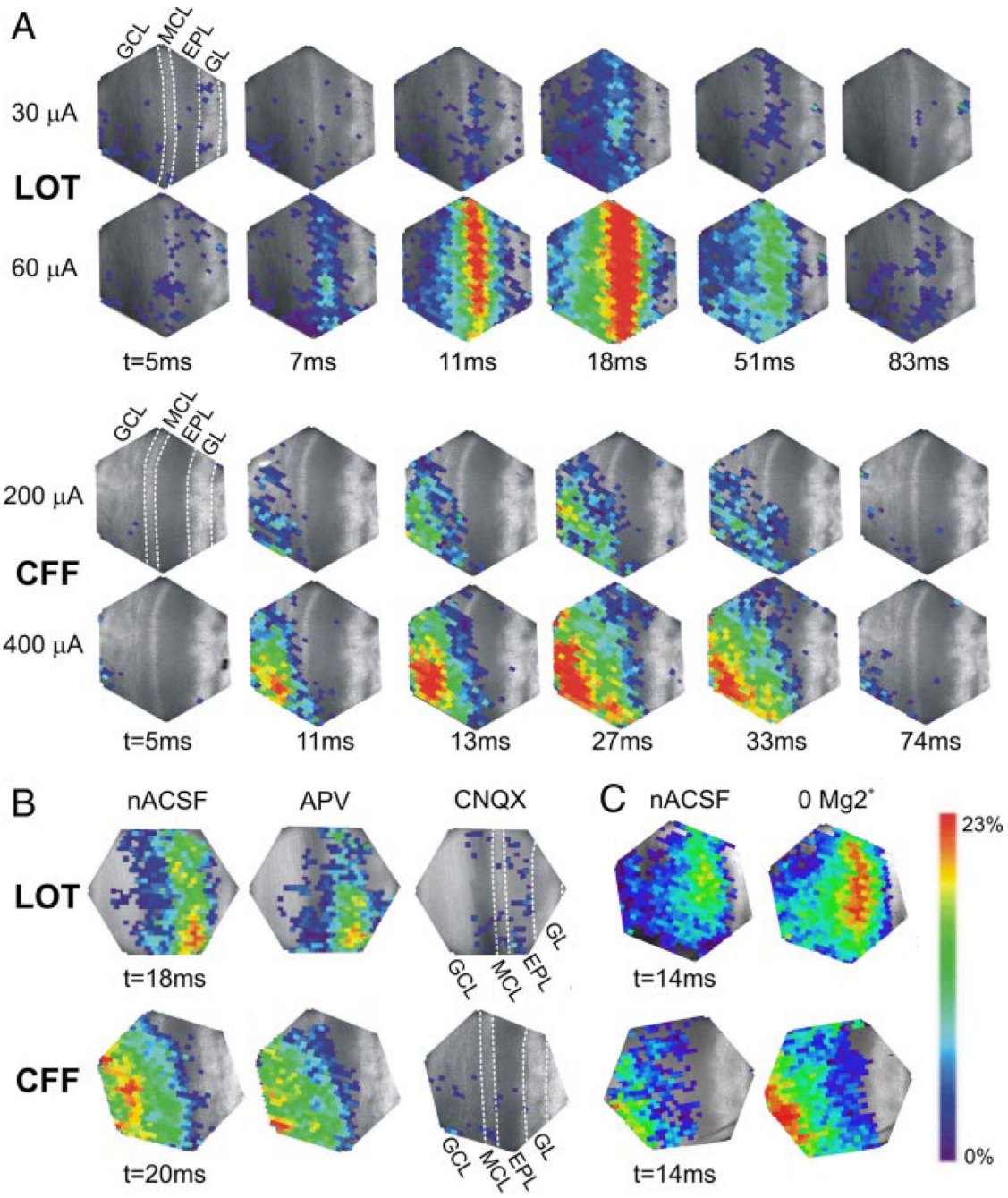

FIG. 3.

Spatiotemporal pattern of optical signals after activation of the LOT (*top 2 rows*) or CFF tract (*bottom 2 rows*). Poststimulus time intervals (*t*, in ms) are shown below each image. *A*, *top*: responses elicited by peri-threshold stimulation intensity (LOT, 30 μA; CFF, 200 μA); *bottom*: responses elicited by 2×-threshold level stimulation intensity (LOT, 60 μA; CFF, 400 μA). *B*: effects of ionotropic glutamate receptor antagonists. *Left*: maximal amplitude and spatial extent of LOT (*top*)- and CFF-evoked (*bottom*) responses in nACSF; stimulation intensity: LOT, 60 μA; CFF, 200 μA. The *N*-methyl-D-aspartate (NMDA) receptor antagonist APV moderately reduced the amplitude and spatial extent of the evoked responses (*middle*), whereas subsequent application of the AMPA receptor antagonist 6-cyano-7-

nitroquinoxalene-2,3-dione (CNQX) nearly completely abolished the responses (*right*). Poststimulus intervals for APV and CNQX are the same as in nACSF. *C*: enhancement of NMDA receptor activity increases LOT (*top*)- and CFF-evoked (*bottom*) responses; stimulation intensity: LOT, 40 μA; CFF, 200 μA. *Left* and *right*, respectively: responses in nACSF and responses after slices were perfused with Mg^{2+}-free ACSF (0 Mg^{2+}). The poststimulus intervals shown (14 ms) correspond to the time of maximal responses in nACSF. Results shown in *A–C* are from different slices.

TABLE 1

Presynaptic and postsynaptic components of field potentials recorded in the granule cell layer evoked by stimulation of the LOT or the centrifugal fiber (CFF) tract

		Postsynaptic Component	
Stimulation Site	**Presynaptic Component Onset Latency**	**Onset latency**	**Duration**
LOT (n = 10)	1.3 ± 0.2 (7)*	7.3 ± 0.8 (10)	27.9 ± 4.1 (10)
CFF (n = 8)	3.5 ± 0.4 (5)	8.2 ± 0.4 (8)	30.8 ± 2.2 (8)

Values are means ± SE of the onset latency in ms. The number of slices in which pre- or postsynaptic responses components were observed is indicated in parentheses.

* Note that presynaptic values for lateral olfactory tract (LOT) stimulation were taken from field potentials recorded in the mitral cell layer/external plexiform layer (MCL/EPL) (see text for details).

TABLE 2

Postsynaptic components of voltage-sensitive dye (VSD) optical responses in different layers of the MOB elicited by suprathreshold LOT or CFF stimulation.

	LAYER		
Stimulation Site	**GL**	**EPL/MCL**	**GCL**
LOT (n = 30)	8.9 ± 0.6 (7)	7.3 ± 0.4 (30)	10.0 ± 0.6 (23)
CFF (n = 27)	11.7 ± 2.4 (4)	10.9 ± 0.8 (18)	6.8 ± 0.5 (27)

All values are means ± SE of the onset latency in ms. The number of slices in which postsynaptic responses were observed are indicated in parentheses. GL, glomerular layer; GCL, granule cell layer.

TABLE 3

Effects of APV and Mg^{2+}-free ACSF

Stimulation Site	Response Type	APV		Mg^{2+}-Free ACSF	
		Amplitude	Half-Width	Amplitude	Half-Width
LOT	FP	–4.4 ± 1.6 (6, *P* = 0.06)	–0.7 ± 0.7 (6, *P* = 0.22)	27.3 ± 6.9 (6, *P* = 0.03)	26.0 ± 9.8 (6, *P* = 0.13)
	OS	–21.9 ± 1.8 (5, *P* = 0.003)	–11.1 ± 6.0 (5, *P* = 0.14)	31.2 ± 8.2 (5, *P* = 0.02)	27.3 ± 8.9 (5, *P* = 0.04)
CFF	FP	–5.6 ± 8.7 (5, *P* = 0.31)	–2.6 ± 5.0 (5, *P* = 0.37)	43.5 ± 14.9 (5, *P* = 0.03)	29.3 ± 13.3 (5, *P* = 0.07)
	OS	–52.2 ± 8.9 (5, *P* = 0.02)	–26.3 ± 9.2 (5, *P* = 0.06)	25.2 ± 6.4 (4, *P* = 0.04)	22.9 ± 4.1 (4, *P* = 0.01)

Effects of the *N*-methyl-D-aspartate receptor antagonist 2-amino-5-phosphonovaleric acid (APV) and Mg^{2+}-free artificial cerebrospinal fluid (ACSF) on the peak amplitude and half-width of field potentials (FPs) and VSD optical signals (OS) elicited by LOT or CFF stimulation. All values are means ± SE percent increase or decrease from control values in normal ACSF. The number of slices and *P* values are indicated in parentheses.